Supplemental material

Mohan et al., https://doi.org/10.1083/jcb.201807124

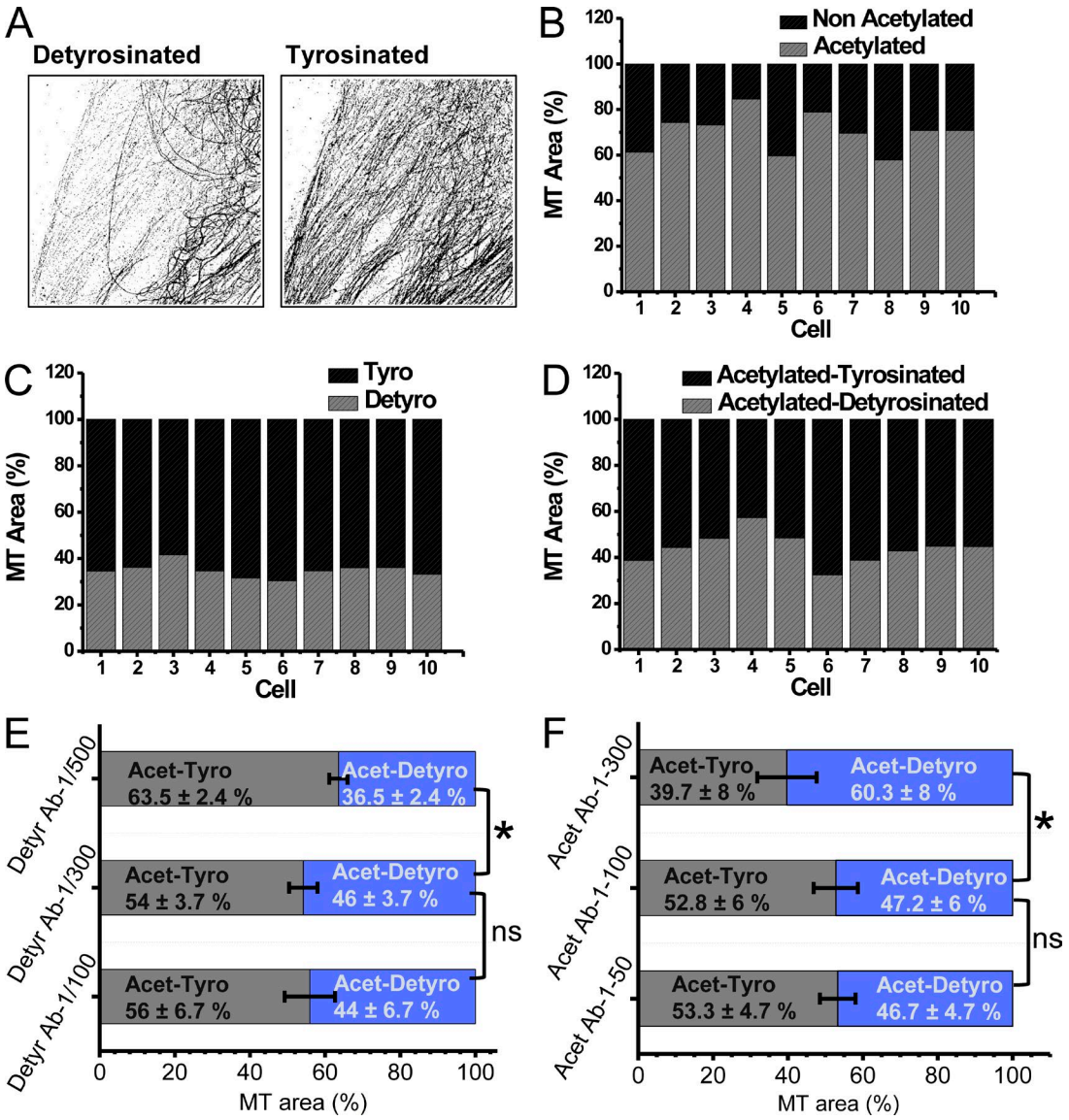

Figure S1. **Quantification of microtubule PTM proportion. (A)** To quantify the proportion of different post-translationally modified microtubules, two-color super-resolution images were converted to binary images, a threshold was applied to remove sparse background pixels while maintaining pixels associated with microtubules, and the total number of pixels belonging to the different modifications was quantified. In the case of detyrosinated and tyrosinated α-tubulin, the pixel values were added to obtain the amount of total tubulin. **(B–D)** Bar plots show the proportion of acetylated, detyrosinated α-tubulin as well as the proportion of acetylated α-tubulin that is also detyrosinated in individual cells. **(E)** Bar plot shows the proportion of acetylated-tyrosinated versus acetylated-detyrosinated microtubules quantified from two-color super-resolution images using a fixed concentration of the antibody against acetylated microtubules (1:100) and varying the concentration of the antibody against the detyrosinated microtubules. The labeling was performed sequentially by labeling the detyrosinated microtubules first followed by the acetylated microtubules. **(F)** Bar plot shows the proportion of acetylated-tyrosinated versus acetylated-detyrosinated microtubules quantified from two-color super-resolution images using a fixed concentration of the antibody against detyrosinated microtubules (1:100) and varying the concentration of the antibody against the acetylated microtubules. The labeling was performed sequentially by labeling the acetylated microtubules first, followed by the detyrosinated microtubules. We used the saturating concentration of antibody (1:100) for both detyrosinated and acetylated microtubules in A, B, C, and D, to determine the proportion of different subpopulation of microtubules. The bars indicate the median, and the error bar is the SD analyzed for 10 different cells in each case. The asterisk indicates the statistical significance and NS indicates no significance for a two-tailed two-sample *t* test (*, $P < 0.05$). Ab, antibody.

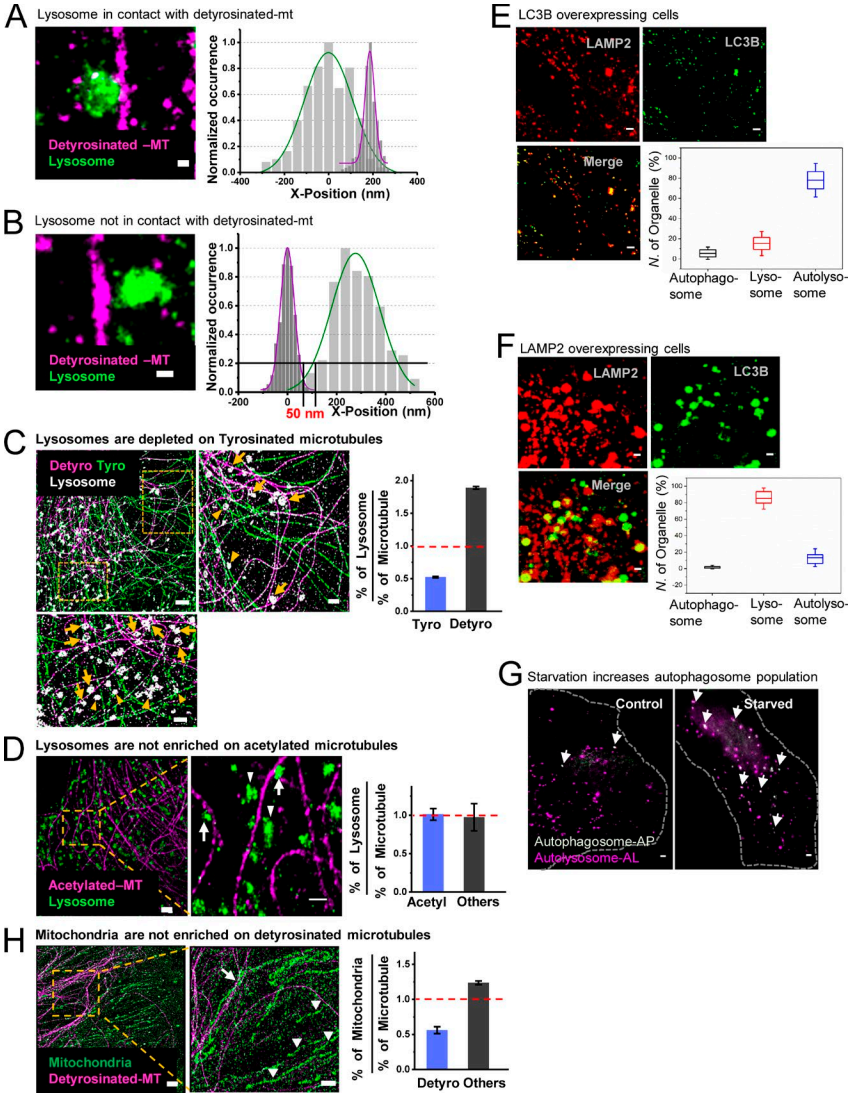

Figure S2. **Lysosomes prefer detyrosinated microtubules. (A and B)** An example of a lysosome that was scored as associated with A or not associated with B, a detyrosinated microtubule. The localizations along the x axis were plotted, and the edges of the lysosome and microtubule were determined by putting a threshold for which the number of localizations was at 20% of the peak value. The edge-to-edge distance was determined, and if this distance was ≥50 nm, the lysosome was considered not to be associated with the microtubule. Bars, 100 nm. **(C)** Three-color super-resolution image of lysosomes (white) and detyrosinated (magenta) and tyrosinated (green) microtubules. Arrows and arrowheads indicate examples of lysosomes associated with detyrosinated and tyrosinated microtubules, respectively. The graph shows quantification of the percentage of lysosomes on tyrosinated (blue) and detyrosinated (gray) microtubules normalized to the overall percentage of the respective microtubule populations. Bars, 2 µm (left) and 1 µm (zooms). The bars and error bars represent the median and SD, respectively, for the three different cells analyzed. The total number of lysosomes analyzed, *n* = 953 (on Tyro = 325, Detyro = 628). **(D)** Two-color super-resolution image of lysosomes (green) and acetylated microtubules (magenta). Arrows and arrowheads indicate examples of lysosomal compartments associated and not associated with acetylated microtubules, respectively. The graph shows quantification of the percentage of lysosomes on acetylated microtubules normalized to the percentage of acetylated microtubules. The bars and error bars represent the median and SD, respectively, for three different cells analyzed. The total number of lysosomes analyzed, *n* = 2,067 (acetylated = 1,459, others = 608). Bars, 1 µm (left) and 500 nm (right). **(E)** LC3B (green) in LC3B-mCherry–overexpressing cells, immunofluorescence image of LAMP2 (red), and overlay. Quantification of the percentage of LC3B-only vesicles (autophagosomes), LAMP2-only vesicles (lysosomes), and LC3B-positive vesicles that are also positive for LAMP2 (autolysosomes). In LC3B-mCherry–overexpressing cells, the majority of vesicles visualized using the LC3B fluorescence were autolysosomes. Bars, 2 µm. **(F)** LAMP2 (red) in LAMP2-mCherry–overexpressing cells, immunofluorescence image of LC3B (green), and overlay. Quantification of the percentage of LC3B-only vesicles (autophagosomes), LAMP2-only vesicles (lysosomes), and LAMP2-positive vesicles that are also positive for LC3B (autolysosomes). In LAMP2-mCherry–overexpressing cells, the majority of vesicles visualized using the LAMP2 fluorescence were lysosomes. **(G)** Wide-field images showing autophagosomes (white) and autolysosomes (magenta) in control cells and cells after starvation expressing the tandem fluorescent-tagged LC3B plasmid. Arrows indicate autophagosomes. The total number of organelles analyzed for control, *n* = 868 (autophagosome = 122, autolysosome = 746) and for the starved condition, *n* = 588 (autophagosome = 268, autolysosome = 320). **(H)** Two-color super-resolution image of mitochondria (green) and detyrosinated microtubules (magenta). Arrows and arrowheads indicate examples of mitochondria associated and not associated with detyrosinated microtubules, respectively. The graph shows quantification of the percentage of mitochondria on detyrosinated microtubules normalized to the overall percentage of detyrosinated microtubules. The bars and error bars represent the median and SD, respectively, for three different cells analyzed. The total number of mitochondria analyzed, *n* = 243 (on Detyro = 47, others = 196). Bars, 4 µm (left) and 1 µm (right).

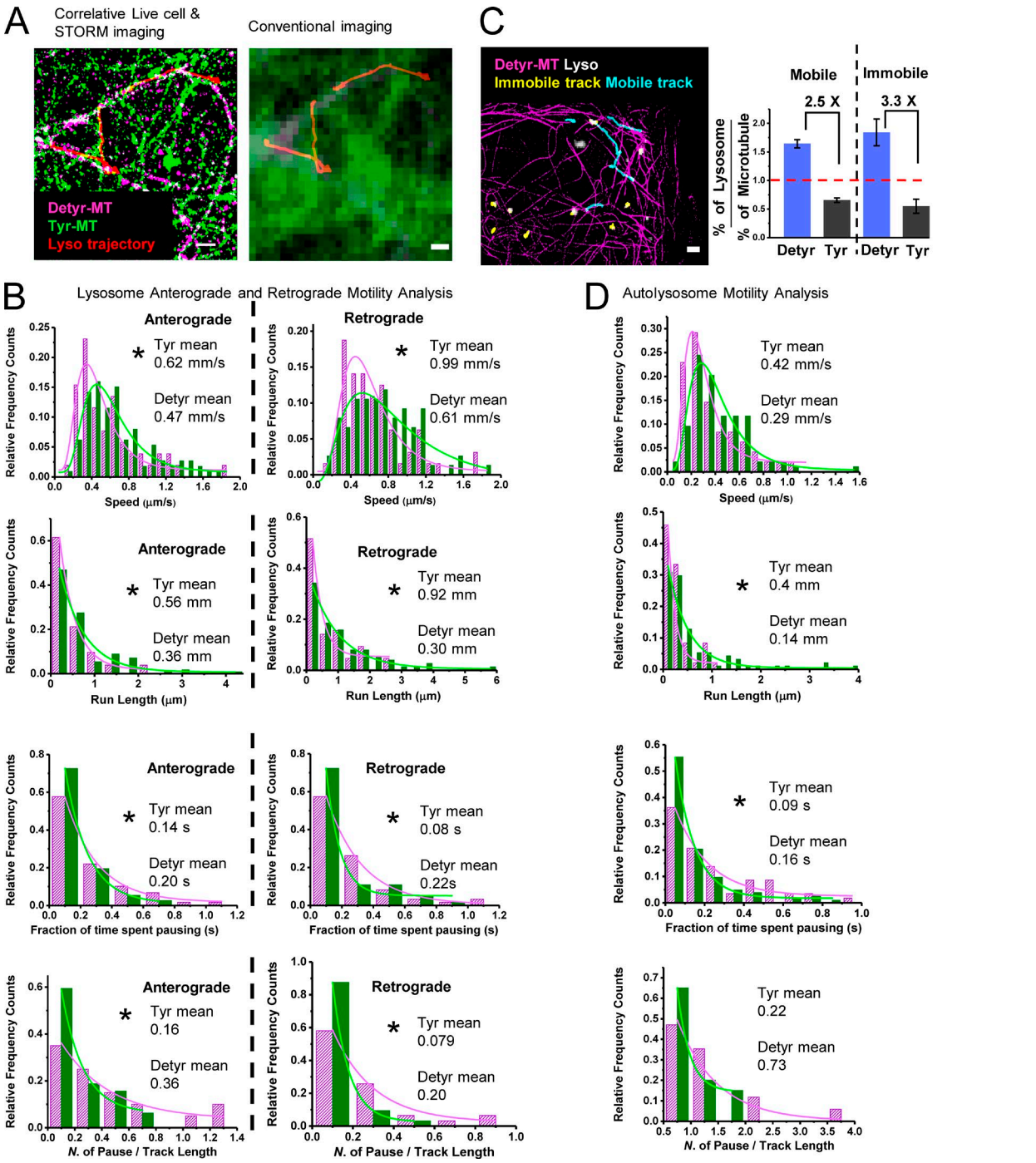

Figure S3. **Motility analysis of lysosomes and autolysosomes on differentially modified microtubules. (A)** The correlative live-cell and super-resolution imaging of lysosome motion on differentially modified microtubules (left) as well as the overlay of trajectories on the conventional image of microtubules (right) to demonstrate the improved resolution and ability to map trajectories to the modified microtubules using correlative imaging. Bars, 500 nm. **(B)** Comparison of speed run length, fraction of time spent pausing, and number of pauses per total track length for lysosomes moving in the antero- or retrograde direction on detyrosinated (magenta) and tyrosinated (green) microtubules. Total number of tracks analyzed, $n = 32$ for tyrosinated anterograde, $n = 32$ for tyrosinated retrograde, $n = 20$ for detyrosinated anterograde, and $n = 31$ for detyrosinated retrograde, from five different cells. **(C)** Lysosome trajectories from correlative live-cell and super-resolution images overlaid on detyrosinated microtubules (magenta) showing mobile (cyan) and immobile (yellow) lysosomes. Bar, 2 µm. The plot shows quantification of the percentage of mobile and immobile lysosomes associated to detyrosinated or tyrosinated microtubules normalized to the overall percentage of the respective microtubule subpopulation. **(D)** Comparison of speed, run length, fraction of time spent pausing, and the number of pauses per total track length for autolysosomes moving on detyrosinated (magenta) and tyrosinated (green) microtubules. Total number of tracks analyzed, $n = 25$ for tyrosinated and $n = 18$ for detyrosinated, from three different cells. The mean speed was estimated from the log-normal fit (solid line) of the data (histogram), and the mean values for the run length, fraction of time spent pausing, and number of pauses per total track length were calculated from the exponential fit (solid line) of the respective data (histograms).The asterisks indicate the statistical significance for the difference in the motility parameter compared for tyrosinated versus detyrosinated populations, for a two-tailed two-sample *t* test (*, $P < 0.05$).

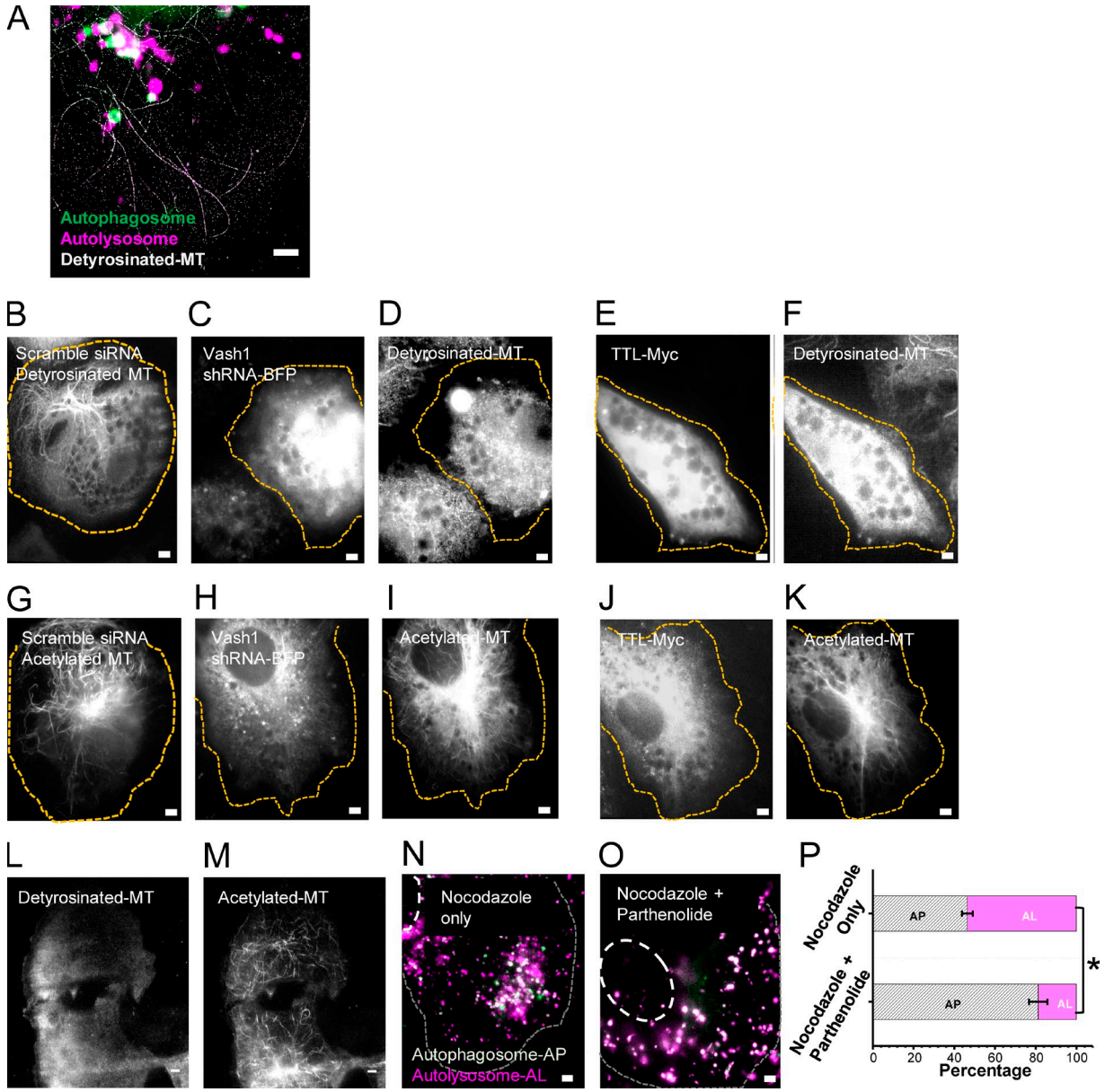

Figure S4. **Lysosome–Autophagosome interactions happen on detyrosinated microtubules. (A)** Heterotypic interactions between autophagosomes (green) and autolysosomes (magenta) predominantly occur on detyrosinated microtubules (white). The region of interest is perinuclear to the periphery of the cell. Bar, 2 µm. **(B–D)** Cells transfected with scrambled or vasohibin 1 (Vash1) shRNA and immunostained for detyrosinated microtubules. (B) Wide-field image showing detyrosinated microtubules in cells transiently transfected with scrambled siRNA (C). Wide-field image showing cells positive for Vash1–BFP fluorescence and (D) detyrosination signal in the corresponding cell, which lacked detyrosinated microtubules. **(E and F)** Cells overexpressing TTL and immunostained for detyrosinated microtubules. (E) Wide-field image showing cells positive for TTL-Myc fluorescence and (F) detyrosination signal in the corresponding cell, which lacked detyrosinated microtubules. Bar, 4 µm. **(G–K)** Cells transfected with scrambled or Vash1 shRNA and immunostained for acetylated microtubules. (G) Wide-field image showing acetylated microtubules in cells transiently transfected with scrambled siRNA. (H) Wide-field image showing cells positive for Vash1–BFP fluorescence and (I) acetylation signal in the corresponding cell, which contained acetylated microtubules. (J and K) Cells overexpressing TTL and immunostained for acetylated microtubules. (J) Wide-field image showing cells positive for TTL-Myc fluorescence and (K) acetylation signal in the corresponding cell, which contained acetylated microtubules. Bar, 4 µm. **(L and M)** Cells were treated with 10 µM nocodazole for 2 h and recovered in complete cell growth media with 10 µM parthenolide for 16 h. (L) Wide-field image showing the depletion of detyrosinated microtubules whereas (M) acetylated microtubules were reformed during the treatment with parthenolide. Bar, 4 µm. **(N and O)** Wide-field image showing autophagosomes (white) and autolysosomes (magenta) in control cells treated with nocodazole only and recovered in the absence of parthenolide (N) or cells after treatment with nocodazole and recovery in the presence of parthenolide (O) expressing the tandem fluorescent-tagged LC3B plasmid. Bar, 2 µm. **(P)** Quantification of the percentage of autophagosomes and autolysosomes for the conditions corresponding to N and O. The asterisk indicates the statistical significance for a two-tailed two-sample *t* test (*, $P < 0.05$).

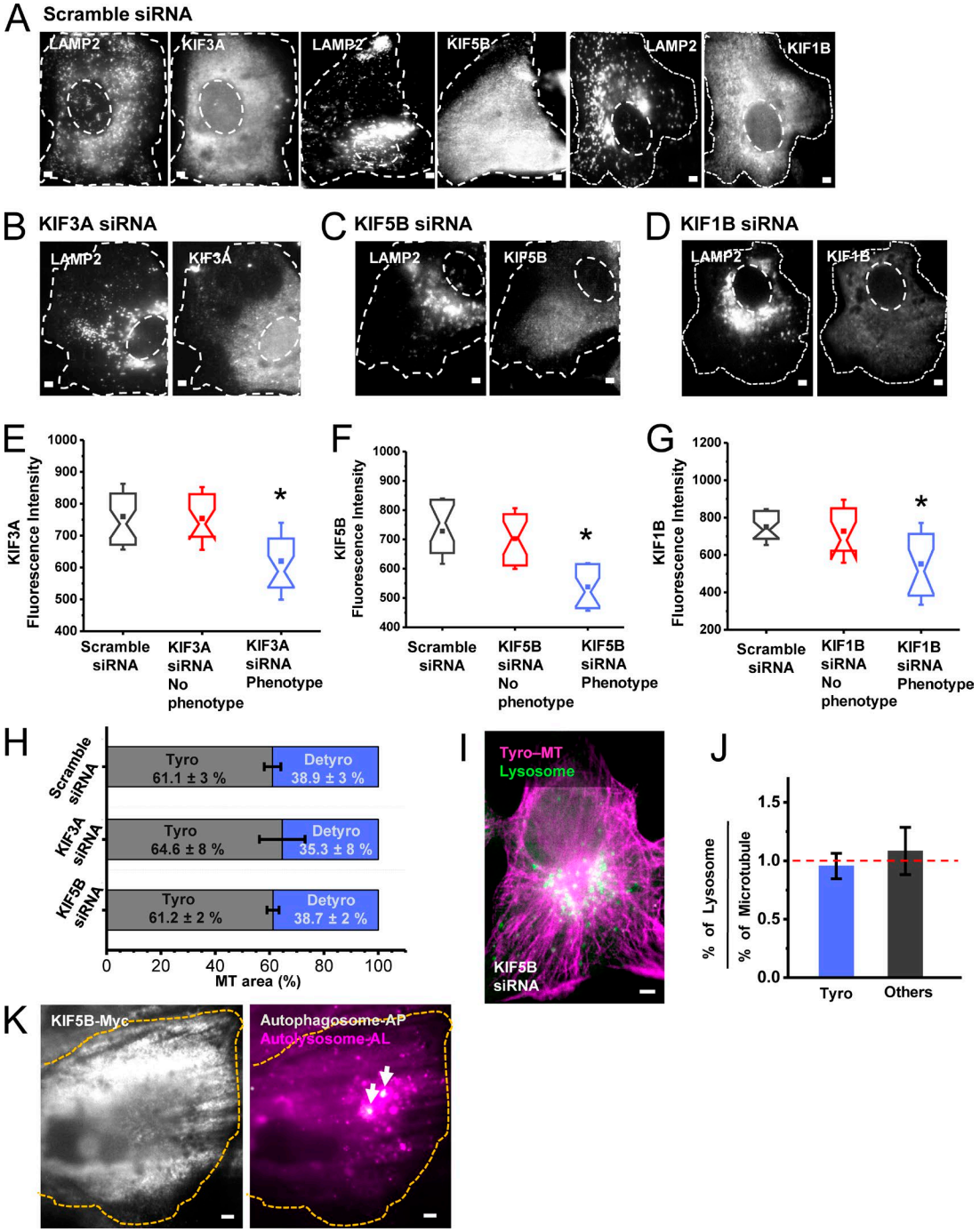

Figure S5. **Kinesin knockdown assay. (A–D)** Cells stably expressing LAMP-2 mCherry, transiently transfected with scrambled siRNA (A), KIF3A siRNA (B), KIF5B siRNA (C), or KIF1B siRNA (D) followed by immunofluorescence for the respective motors. The scrambled siRNA–transfected cells show the typical lysosome distribution (LAMP-2) throughout the cell, with some clustering around both the perinuclear region and the cell periphery, whereas KIF3A, KIF5B, and KIF1B knockdown leads to the phenotype of lysosomes clustered in the perinuclear region with few lysosomes toward the cell periphery. **(E–G)** KIF3A (E), KIF5B (F), and KIF1B (G) fluorescence intensities were quantified from immunofluorescence and were compared among cells transfected with scrambled siRNA (black), cells transfected with KIF3A, KIF5B, or KIF1B siRNA that did not show the perinuclear clustering phenotype (red) or cells transfected with KIF3A, KIF5B, or KIF1B siRNA that showed the perinuclear clustering phenotype (blue). **(H)** Bar plots show the proportion of detyrosinated and tyrosinated α-tubulin for the cells transfected with scrambled, KIF3A, or KIF5B siRNA. The bars indicate the median, and the error bar is the SD analyzed for five different cells in each case. **(I and J)** Quantification of lysosome association to tyrosinated microtubules after KIF5B knockdown. (I) Wide-field image showing lysosomes (green) and tyrosinated microtubules (magenta) after KIF5B knockdown. (J) The graph shows quantification of the percentage of lysosomes on tyrosinated microtubules quantified from two-color super-resolution images and normalized to the overall percentage of tyrosinated microtubules. The bars and error bars represent the median and SD, respectively, for three different cells analyzed. The total number of lysosomes analyzed, n = 322 (on Tyro = 198, others = 124). **(K)** Wide-field images showing the overexpressed KIF5B, which was labeled with a Myc-tag (left) and the autophagosomes (white) and autolysosomes (magenta) in the corresponding cell (right). The asterisks indicate the statistical significance for the difference in the motility parameter compared for tyrosinated versus detyrosinated populations, for a two-tailed two-sample t test (*, $P < 0.05$). Bars, 2 µm.

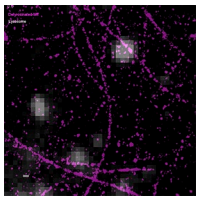

Video 1. **Correlative live-cell and STORM imaging of lysosome moving on detyrosinated microtubules.** Associated with Fig. 4, A–D.

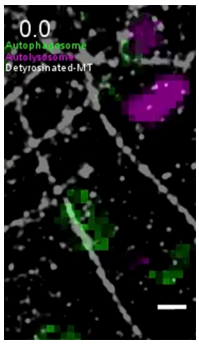

Video 2. **Correlative live-cell and STORM imaging of autophagosome–lysosome interactions on detyrosinated microtubules.** Associated with Fig. 5 A.

Table S1. **siRNAs used in this study**

siRNA	Part number	Sequence (5′–3′)	Vendor and description
KIF5B (1)	Custom-synthesized	AUGCAUCUCGUGAUCGCAADTDT	Sigma-Aldrich
		UGAAUUGCUUAGUGAUGAATT	*Homo sapiens* KIF5B
		UCAAGUCAUUGACUGAAUATT	Custom synthesized pool
KIF5B (2)	L-008867-00-0005	GAACUGGCAUGAUAGAUGA	Dharmacon
		CAACAGACAUGUAGCAGUU	ON-TARGETplus Human KIF5B (3799) siRNA-SMARTpool
		GCAGGAACGUAUAAGAGUA	
		CAAUUGGAGUUAUAGGAAA	
KIF1B	L-009317-00-0005	AAACAGAGGCCAUCAGAAU	Dharmacon
		CUUAUACAAUGAUGGGUAA	ON-TARGETplus Human KIF1B (23095) siRNA-SMARTpool
		CAAAGGGACUCGAUUAAAG	
		GAAAUGGAGAUCUUAUACA	
KIF3A	4390824	Sense: CUAUCAGUACAUUACGGUATT	Thermo Fisher Scientific
		Antisense: UACCGUAAUGUACUGAUAGTT	*H. sapiens* kinesin family member 3A (s21942)
Scrambled	4390846		Thermo Fisher Scientific
			Select Negative Control No. 2 siRNA
Vasohibin shVASH1	Custom-made	Target: GGGAATTTACCTCACCAACAG	Custom-made
		Full sequence: GGGAATTTACCTCACCAA CAGCGAACTGTTGGTGAGGTAAATTCCC	University of Pennsylvania

Table S2. **Antibodies used in this study**

Antibody	Host species	Catalog number	Vendor
α-Tubulin	Rabbit	ab18251	Abcam
Detyrosinated α-tubulin	Rabbit	ab48389	Abcam
Tyrosinated α-tubulin	Mouse	MAB1864-I	EMD Millipore
Acetylated α-tubulin	Mouse	T6793	Sigma-Aldrich
mCherry	Chicken	nbp2-25158	Novus Biologicals
MYC-tag	Rabbit	16286-1-AP	Proteintech
MYC-tag	Mouse	60003-2-Ig	Proteintecho
GFP	Chicken	ab13970	Abcam
DsRed	Mouse	200-301-379	Rockland
LAMP1	Rabbit	ab24170	Abcam
LAMP1	Mouse	15665S	Cell Signaling
LAMP2	Rabbit	H4B4-s	Developmental Studies Hybridoma Bank
LC3B	Rabbit	L7543	Sigma-Aldrich
Tom20	Mouse	Sc-17764	Santa Cruz Biotechnology
KIF1B	Rabbit	15263-1-AP	Proteintech
KIF5B	Rabbit	21632-1-AP	Proteintech
KIF3A	Mouse	Ab24626	Abcam